Supporting Information:

Ultralow Temperature Solution-Processed Aluminum-Oxide Dielectrics via Local Structure Control of Nanoclusters

Jeong-Wan Jo[1†], Yong-Hoon Kim[2†], Joohyung Park[3], Jae Sang Heo[1], Seongpil Hwang[4], Won-June Lee[5], Myung-Han Yoon[5], Myung-Gil Kim[3], and Sung Kyu Park[1*]*

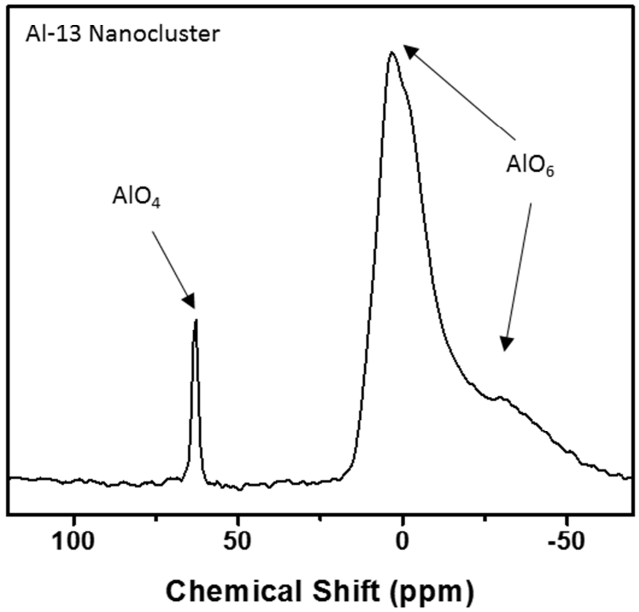

Figure S1. ^{27}Al MAS NMR spectrum of the nanocluster-aluminum precursor powder obtained by evaporating the nanocluster-aluminum precursor solution (solvent: 2-methoxyethanol)

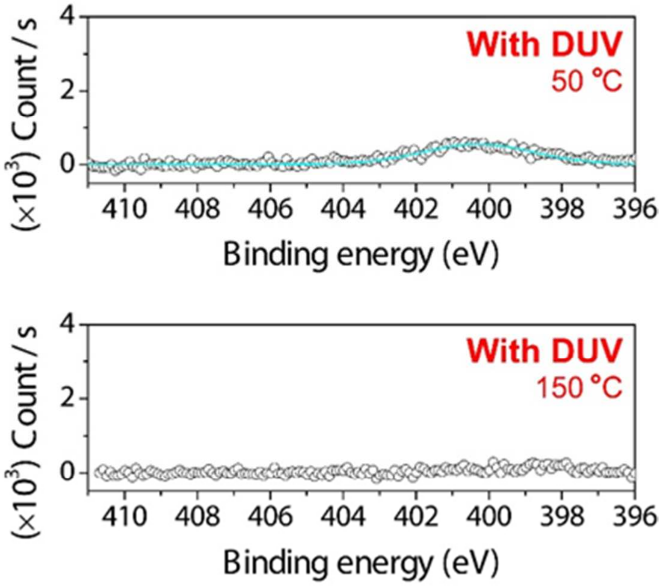

Figure S2. N1s XPS spectra of DUV activated aluminum oxide films. The DUV activation was carried out at temperatures of 50 and 150 °C.

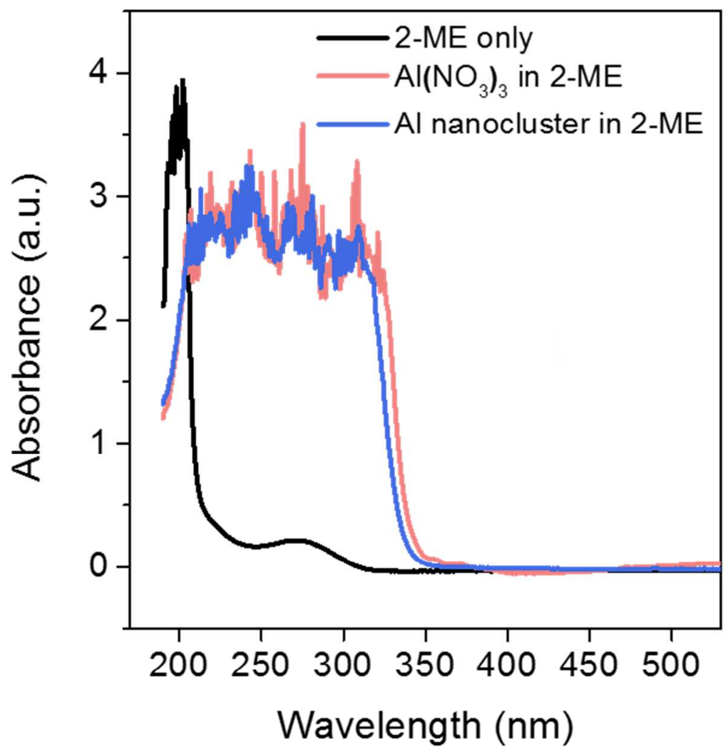

Figure S3. Light absorption characteristics of 2-ME, aluminum nitrate solution, and aluminum nanocluster solution.

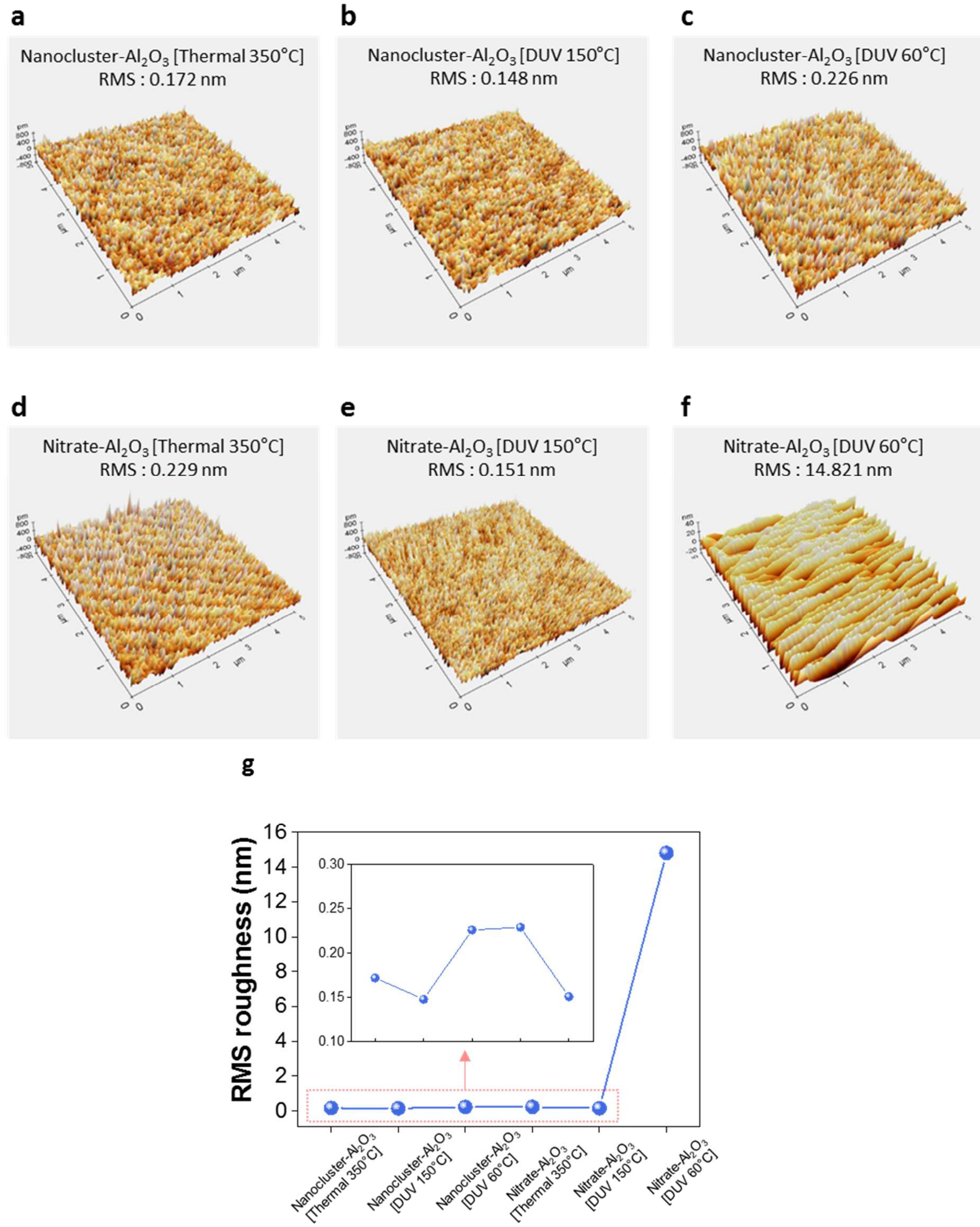

Figure S4. AFM images of nanocluster- and nitrate-Al_2O_3 films. AFM images of nanocluster-Al_2O_3 films annealed by (a) thermal 350 ˚C, (b) DUV 150 ˚C and (c) DUV 60 ˚C. AFM images of nitrate-Al_2O_3 films annealed by (d) thermal 350 ˚C, (e) DUV 150 ˚C and (f) DUV 60 ˚C. (g) RMS surface roughness of nanocluster- and nitrate-Al_2O_3 films (Thermal 350 ˚C, DUV 150 ˚C and DUV 60 ˚C).

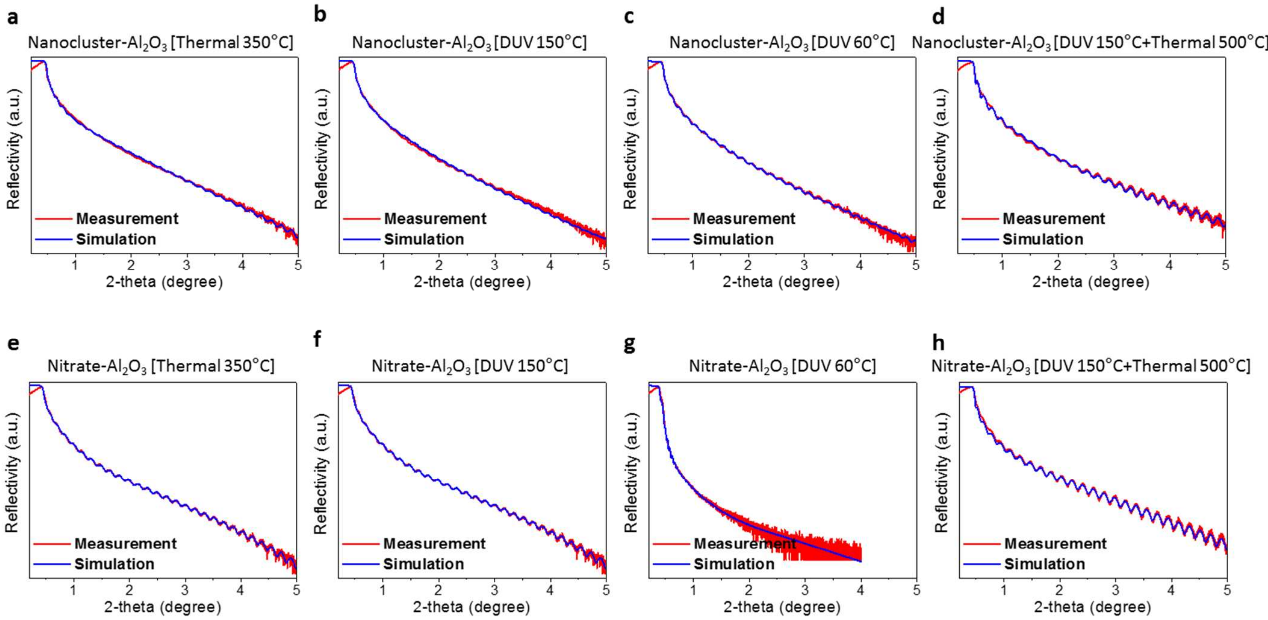

Figure S5. X-ray reflectivity (XRR) spectra of alumina thin films. XRR data and corresponding fitted data as a function of 2-theta: nanocluster-Al_2O_3 films annealed by (a) thermal 350 ˚C, (b) DUV 150 ˚C, (c) DUV 60 ˚C and (d) DUV 150 ˚C + thermal 500 ˚C. nitrate-Al_2O_3 films annealed by (e) thermal 350 ˚C, (f) DUV 150 ˚C, (g) DUV 60 ˚C and (h) DUV 150 ˚C + thermal 500 ˚C.

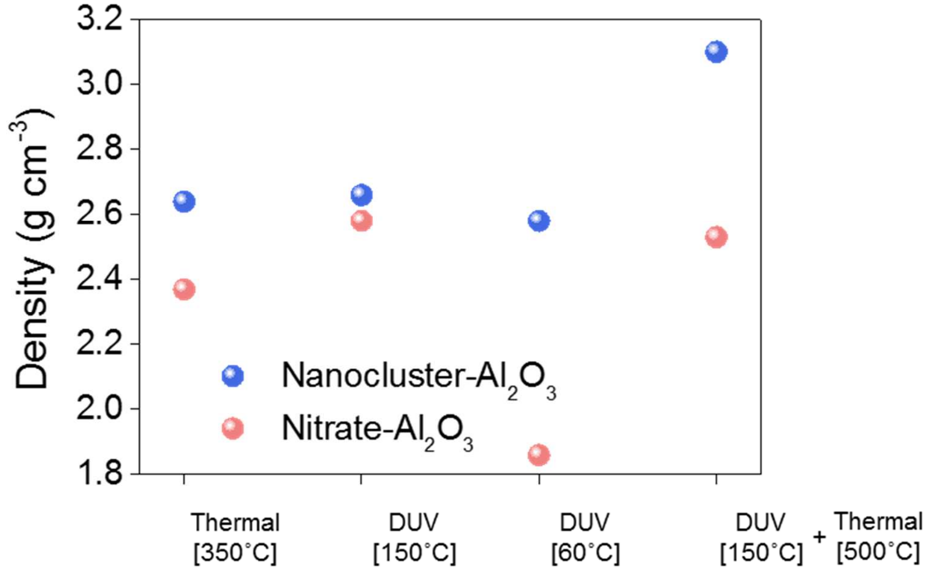

Figure S6. Bulk film densities of nanocluster- and nitrate-Al_2O_3 films depending on the annealing condition (Thermal 350 ˚C, DUV 150 ˚C, DUV 60 ˚C, DUV 150 ˚C + Thermal 500 ˚C). The data were obtained from XRR data.

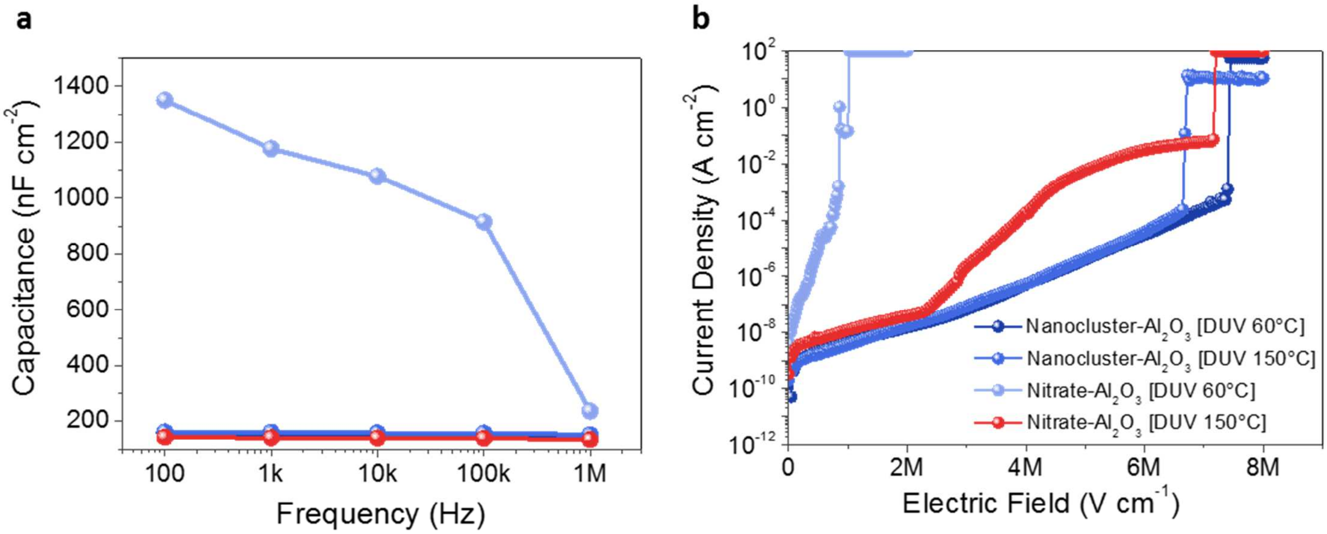

Figure S7. Gate dielectric properties of nanocluster- and nitrate-Al_2O_3 films. (a) C-F and (b) J-E characteristics of nanocluster- and nitrate-Al_2O_3 gate dielectrics annealed by DUV 60 ˚C and DUV 150 ˚C.

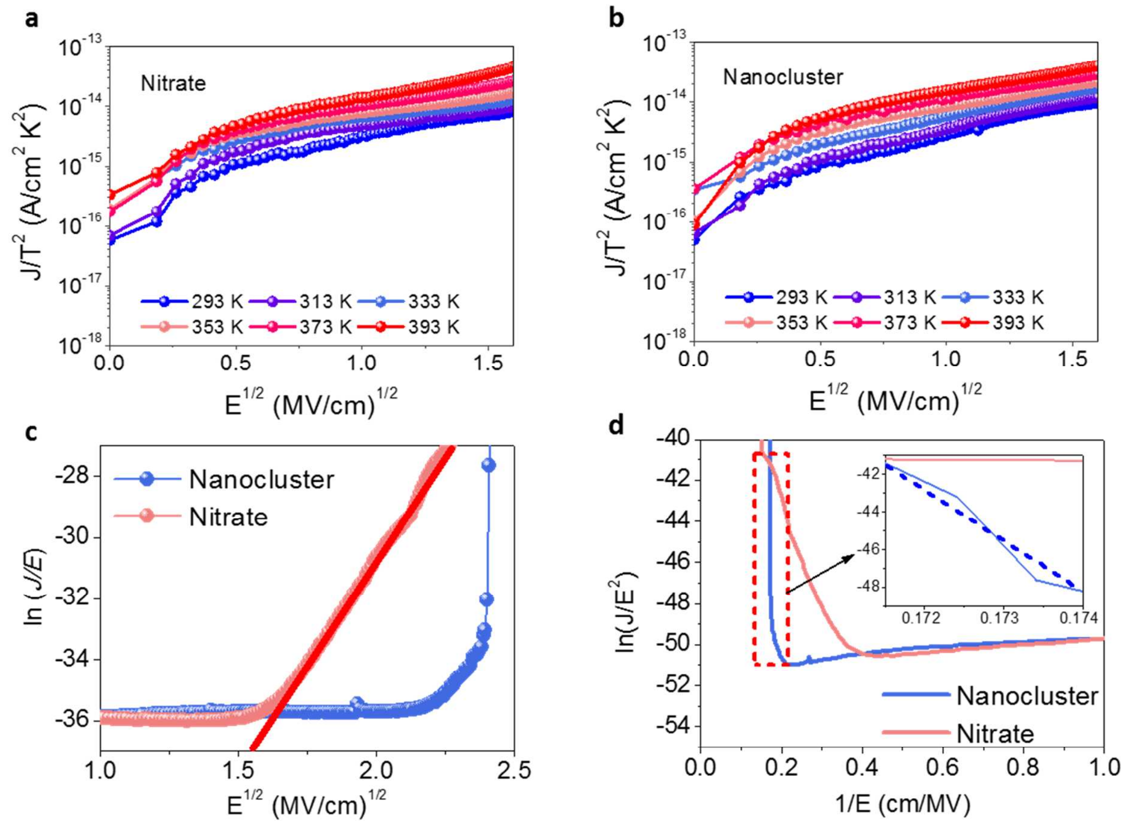

Figure S8. (a) and (b) J/T^2 versus $E^{1/2}$ curves revealing a Schottky emission region, (c) ln (J/E) versus $E^{1/2}$ curves revealing a Poole-Frenkel emission region, and (d) $\ln(J/E^2)$ versus 1/E curves revealing an F-N tunneling region in which the plot was fitted to an apparent linear curve of the F-N tunneling equation.

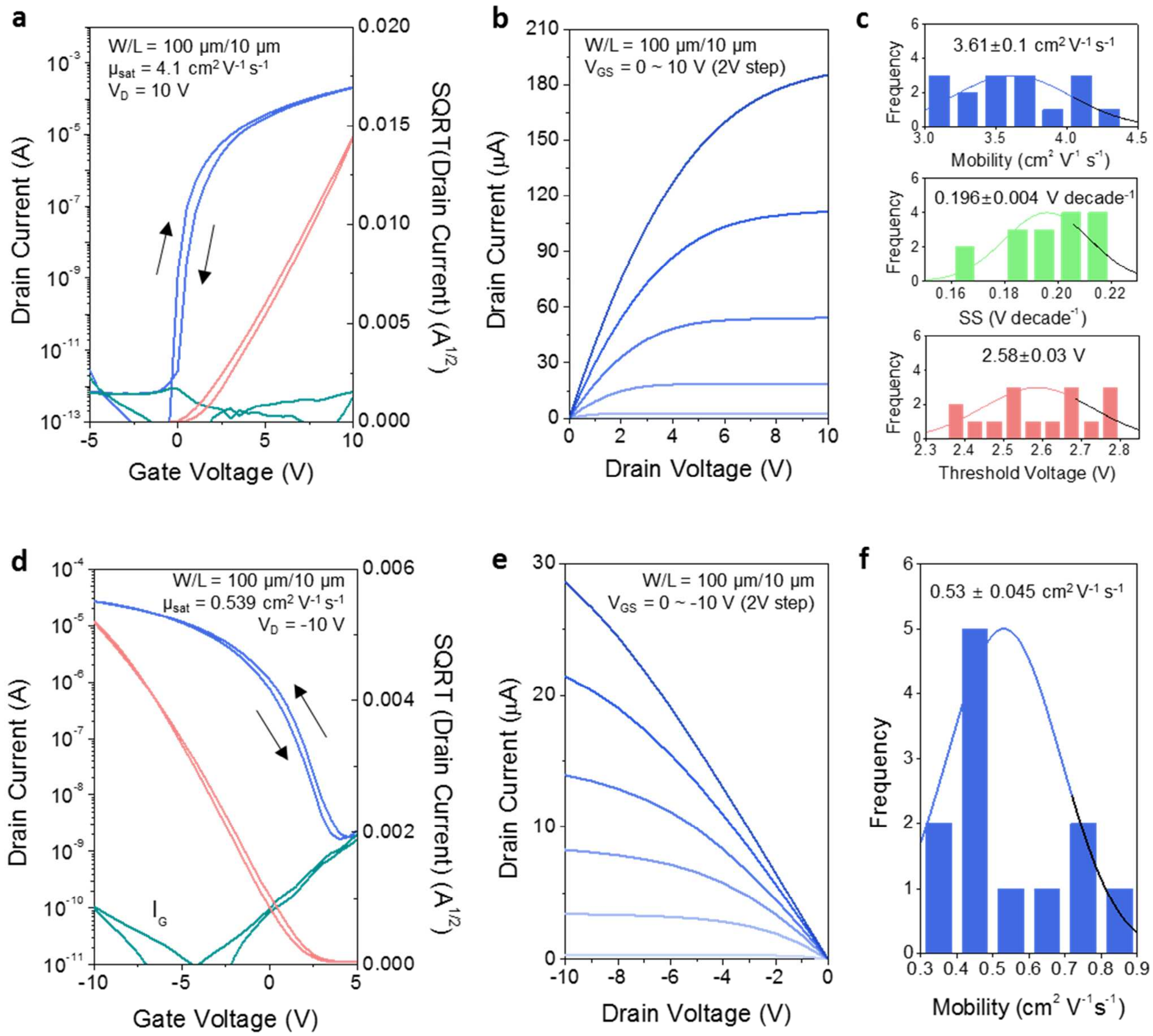

Figure S9. Electrical characteristics of *a*-IGZO and CNT TFTs using ultralow-temperature-annealed nanocluster-Al_2O_3 gate dielectrics (60 ˚C). (a) Transfer and (b) output characteristics of *a*-IGZO TFTs with an ultralow-temperature-annealed nanocluster-Al_2O_3 gate dielectric (T_{anneal} = 60 ˚C). (c) A statistical distribution of saturation mobility, subthreshold swing (SS), and threshold voltage (V_T) of IGZO TFTs on glass. (d) Transfer and (e) output characteristics of CNT TFTs with an ultralow-temperature-annealed nanocluster-Al_2O_3 gate dielectric (T_{anneal} = 60 ˚C). (f) A statistical distribution of saturation mobility of CNT TFTs.

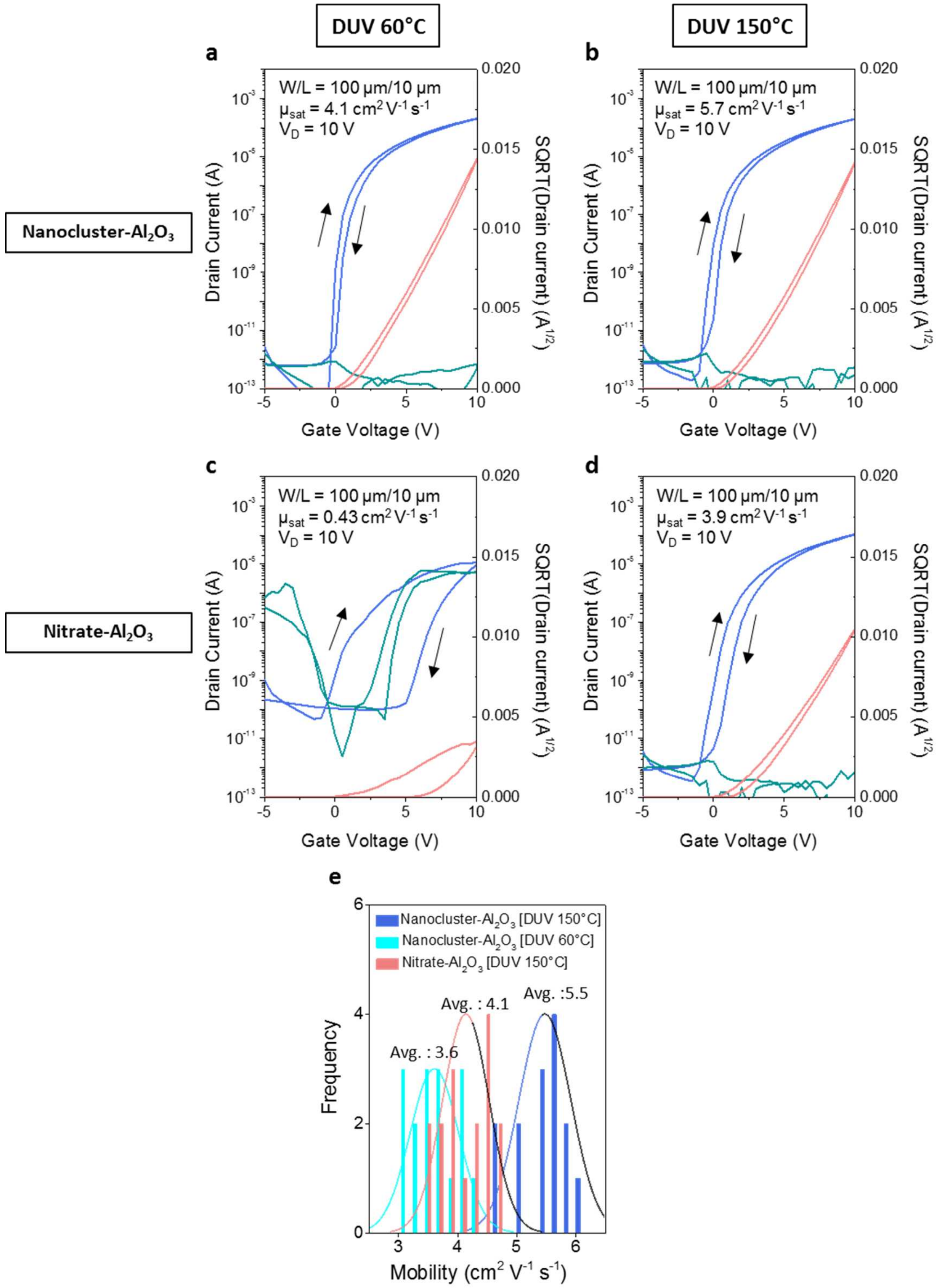

Figure S10. Electrical characteristics of *a*-IGZO TFTs with nanocluster- and nitrate-Al_2O_3 gate dielectrics fabricated on glass substrates. (a-d) Transfer characteristics of *a*-IGZO TFTs with nanocluster- and nitrate-Al_2O_3 gate dielectrics annealed by DUV 60 ˚C and DUV 150 ˚C. (e) A statistical distribution of field-effect mobility for *a*-IGZO TFTs with various gate dielectrics.

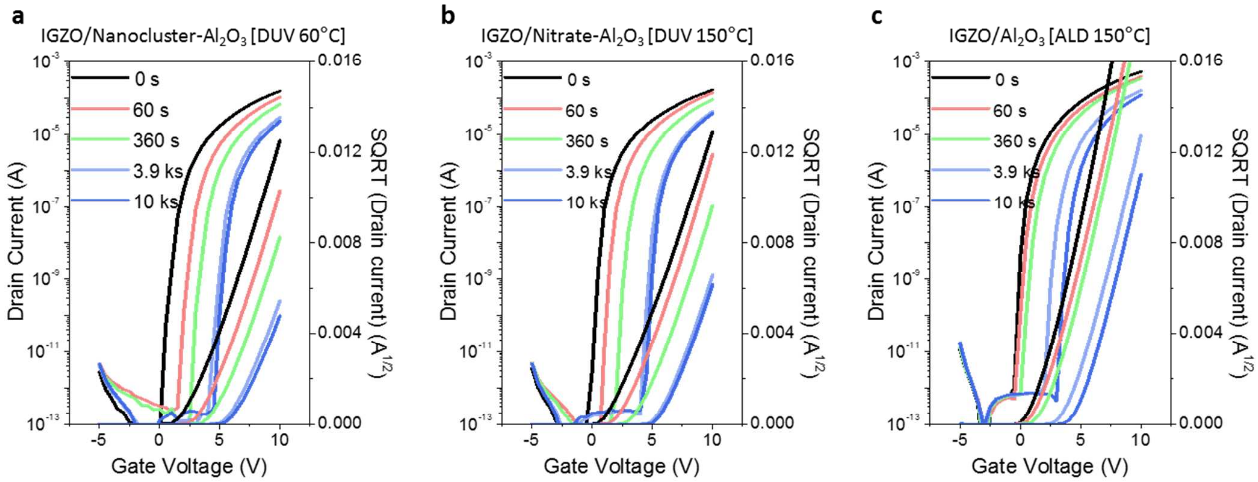

Figure S11. Positive gate-bias stress (PBS) data for flexible *a*-IGZO TFTs with various alumina gate dielectrics (V_{GS} = +5 V, t = 10 ks). *a*-IGZO TFTs with, (a) nanocluster-Al_2O_3 gate dielectric DUV-annealed at 60 ˚C, (b) nitrate-Al_2O_3 gate dielectric DUV-annealed at 150 ˚C and (c) Alumina gate dielectric deposited by ALD at 150 ˚C. All samples were un-passivated and fabricated on PI substrates.

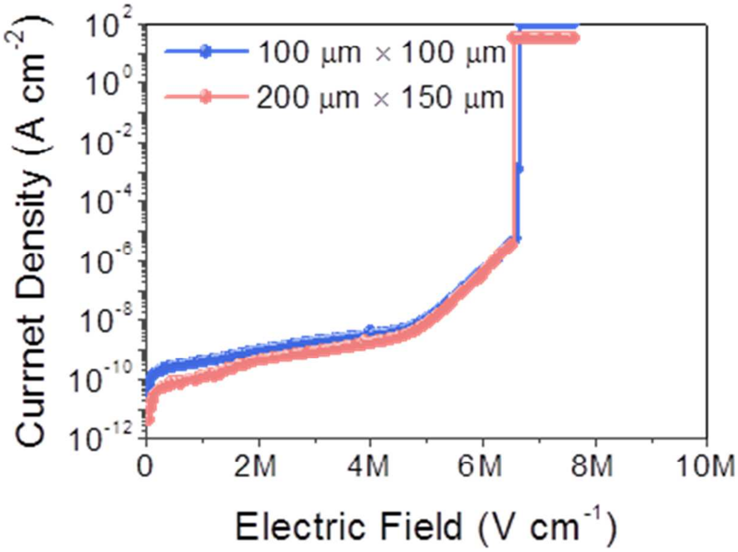

Figure S12. J-E characteristics of nanocluster alumina gate dielectrics with different electrode dimensions.

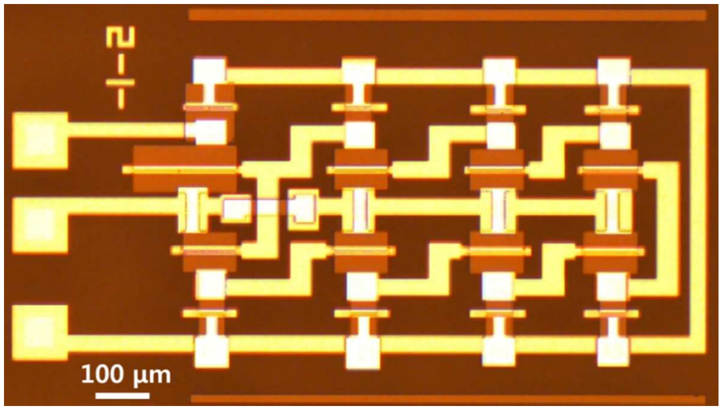

Figure S13. An optical microscope image of a 7-stage ring oscillator using IGZO TFTs with nanocluster alumina gate dielectric.

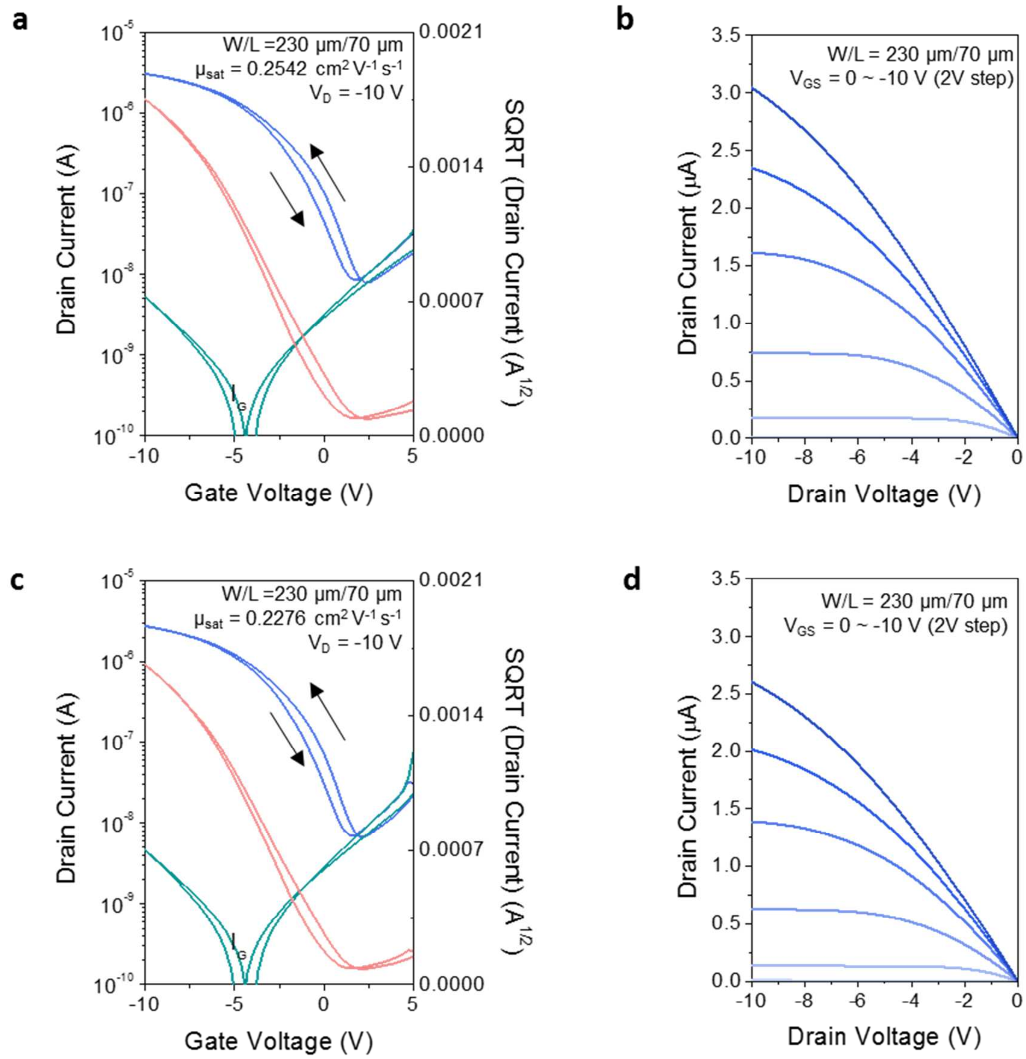

Figure S14. Electrical characteristics of CNT TFTs with nanocluster-Al_2O_3 gate dielectrics fabricated on PU substrates. (a-d) Transfer and output characteristics of CNT TFTs with nanocluster-Al_2O_3 gate dielectrics annealed by DUV 60 ˚C on PU substrate.

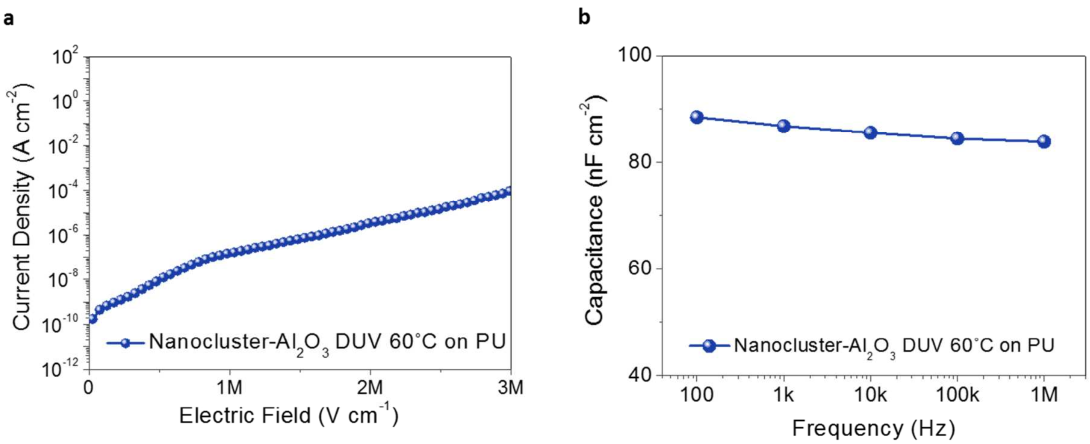

Figure S15. Gate dielectric properties of nanocluster-Al_2O_3 film directly fabricated on PU substrate. (a) J-E and (b) C-F characteristics of nanocluster-Al_2O_3 gate dielectrics annealed by DUV 60 ˚C on PU substrate.

Dielectric	M-O (~531 eV)	M-OH (~532.3 eV)
Nanocluster-Al_2O_3 [Thermal 350°C]	82.4 %	17.6 %
Nanocluster-Al_2O_3 [DUV 150°C]	87.8 %	12.2 %
Nanocluster-Al_2O_3 [DUV 60°C]	85.0 %	15.0 %
Nitrate-Al_2O_3 [Thermal 350°C]	79.3 %	20.7 %
Nitrate-Al_2O_3 [DUV 150°C]	83.7 %	16.3 %
Nitrate-Al_2O_3 [DUV 60°C]	24.1 %	75.9 %

Table S1. Tabulated XPS (O1s) results of nanocluster- and nitrate-Al_2O_3 films. The areal ratios of M-O and M-OH bonding in nanocluster- and nitrate-Al_2O_3 films annealed under different conditions.